Design and Testing of a Simple, Compact Antenna with Reconfigurable Broadside and Monopole-Like Patterns

Ming-Chun Tang, *Senior Member, IEEE*, Yingjie Chen, *Student Member, IEEE*, Xiaoming Chen, *Student Member, IEEE*, Dongmei Mu, and Richard W. Ziolkowski, *Life Fellow, IEEE*

***Abstract*—A compact antenna with broadside and monopole-like pattern reconfigurability is presented. Its radiating elements are linearly polarized and consist of a magnetic dipole and an electric monopole. A capacitively loaded loop (CLL) and two rectangular strips, one driven and one parasitic, serve as a magnetic near-field resonant parasitic radiator. The broadside pattern is generated by the magnetic radiator; the electric monopole radiates the monopole-like pattern. A coax-fed structure is developed with only two PIN diodes integrated into it that dynamically controls the excitation of either the magnetic or the electric radiator. A prototype was fabricated and tested. The measured results are in reasonable agreement with their simulated ones. The antenna is impedance matched within an overlapping operational fractional bandwidth of 3.8%; the combination of its radiating elements is compact with $ka_{rad} = 0.69$. The realized gain value of the broadside pattern at boresight is 7.1 dBi and the null of the monopole-like pattern is over -28 dBi deep. The prototype is an attractive candidate for applications in many space-limited wireless systems that require reconfigurable broadside and monopole-like performance characteristics.**

***Index Terms*—Broadside pattern, monopole-like pattern, near-field resonant parasitic elements, reconfigurable antenna**

I. Introduction

Reconfigurable antennas with broadside and monopole-like radiation pattern diversity exhibit unique performance characteristics. With an ability to electrically switch their patterns they not only provide significantly enhanced coverage, but they also avoid interference arising from noise sources [1-15]. Benefiting from these advantageous features, they have been extensively employed in many modern wireless systems, e.g., radar [1-3], direction-finding [4], anti-interference [5], indoor wireless communications [6-9], global positioning (GPS) [10-11], base station [12], and MIMO (multiple-input–multiple-output) [13-15] systems. As a common method to accomplish their broadside and monopole-like radiation pattern reconfigurability, array antennas have been adopted to switch their patterns between sum and difference ones by controlling the phase differences between each radiator element [1-3, 7]. While effective, the number of radiating elements in those arrays exhausts a significant amount of space [7]. Moreover, these arrays require phase shifters [2], couplers [3] or comparators [1], which significantly increase the system complexity and cost.

Different methods to achieve broadside and monopole-like radiation pattern diversity while simplifying the configuration, saving space, and reducing costs have been developed in recent years. They can be classified into three general categories. The first one deals with reconfiguring the radiators. For example, one could employ PIN diodes to short the elements of a patch array to their ground plane [5, 14, 16, 17]. The second one considers reconfigurable feeding networks, i.e., developing dynamically controlled current pathways beneath the radiators of an array [4, 9, 11, 18]. The third one introduces switchable exciting ports, i.e., broadside and monopole-like radiation patterns are obtained simply by switching the two ports of the system between in-phase and out-of-phase states [12, 19, 20, 21] or by exciting only one of the two ports [6, 8, 10] or several others [13, 15]. Nevertheless, most of these reported designs have unavoidable large electrical sizes that are not suitable for space-limited platform applications. Thus, it is highly desired to achieve a compact antenna with reconfigurable broadside and monopole-like radiation patterns.

In this letter, a broadside and monopole-like pattern-reconfigurable compact antenna is reported. It systematically combines one reconfigurable exciting structure and two orthogonally oriented radiating elements. One is a magnetic radiator for the broadside pattern and the other is an electric monopole element for the monopole-like pattern. Its reconfigurability relies on only 2 PIN diodes switches integrated into its exciting structure. This prototype was tested and the measured results, in agreement with their simulated values in both states, demonstrates that this pattern-reconfigurable antenna can dynamically realize either a stable broadside or monopole-like (with high-level null depth)

Manuscript received on 04, February, 2020; revised on 23, February, 2020; accepted on 14, March, 2020.

This work was supported in part by the National Natural Science Foundation of China contract number 61922018, the Funding of the Innovative Leading Talents in Science and Technology of Chongqing contract number CSTCCXLJRC201705, in part by the Chongqing Natural Science Foundation contract number cstc2019jcyjjqX0004, and in part by the Australian Research Council grant number DP160102219.

M. -C. Tang, Y. Chen, and X. Chen are with the Key Laboratory of Dependable Service Computing in Cyber Physical Society Ministry of Education, School of Microelectronics and Communication Engineering, Chongqing University, Chongqing 400044, China (e-mail: tangmingchun@cqu.edu.cn);

D. Mu is with the School of Electronic Engineering, Beijing University of Posts and Telecommunications, Beijing, 100876, China;

R. W. Ziolkowski is with the University of Technology Sydney, Global Big Data Technologies Centre, Ultimo NSW 2007, Australia (e-mail: richard.ziolkowski@uts.edu.au).

realized gain pattern over the same frequency range.

II. Antenna Geometry

The configuration of the pattern-reconfigurable compact antenna design is presented in Fig. 1. It consists of two radiating elements, an electric one and a magnetic one. Each is etched on a semi-circular disk of Rogers 4350b, whose relative dielectric constant is $\varepsilon_r = 3.48$ and loss tangent is $\tan\delta = 0.0037$. Both substrates, labeled Sub_1 and Sub_2, are vertically placed on and orthogonal to a circular substrate labeled as Sub_3. They have the same thickness, $h_3 = 0.508$ mm, and the same radius $R_2 = 21.0$ mm. The electric radiator is a curved Egyptian axe-shaped electric monopole. The magnetic radiator is an evolved form of the CLL-based near-field resonant parasitic (NFRP) antennas introduced in [22, 23]. Each radiator is driven independently by the same reconfigurable exciting structure printed on Sub_3. The whole antenna system is mounted on a large circular copper disc that acts as its ground plane; it has the thickness $h_5 = 1.0$ mm and radius $R_1 = 96.0$ mm. The optimized design parameters are given in Table I. The electrical size of the main radiators, i.e., the combination of the NFRP and dipole elements alone without the ground plane, is $ka_{rad} = kR_2 = 0.69$ at the resonance frequency, 1.57 GHz.

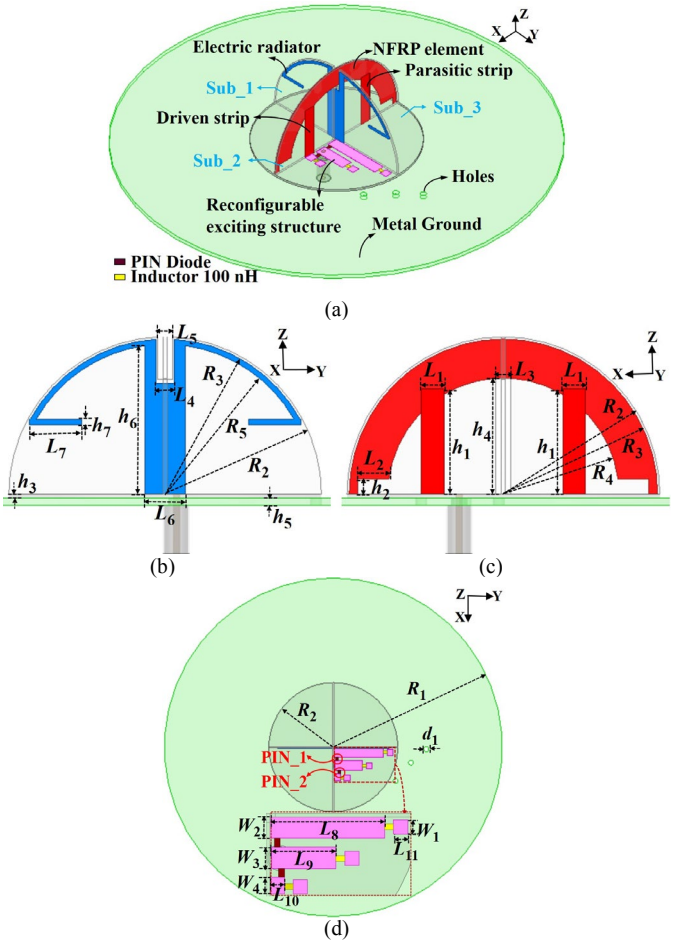

Fig. 1 Geometry of the reported pattern reconfigurable antenna. (a) 3D view. (b) y-z plane. (c) x-z plane. (d) x-y plane.

As shown in Fig. 1(b), the electric radiator is etched on Sub_1 and is directly connected to one strip of the exciting structure on Sub_3 [24]. When this monopole structure is excited, a deep null is achieved at boresight as expected [25]. Note that two straight horizontal arms are introduced at the ends of the curved top strip of the monopole to provide a fine tuning mechanism for the resonance frequency and for impedance matching (see Section III).

As shown in Fig. 1(c), the magnetic radiator consists of one CLL element and two rectangular strips on opposite sides of Sub_2. One strip is connected to a second strip of the exciting structure on Sub_3, which lies orthogonal to it. The other is a parasitic strip that is positioned symmetrically with respect to it in terms of the yoz-plane. It is introduced to guarantee a relatively symmetrical radiation pattern (see Section III). Note that there are two rectangular slits etched at the lower ends of the CLL element to provide another resonance frequency adjustment mechanism. When this magnetic NFRP element is excited, a broadside radiation pattern is generated [22].

The exciting structure is shown in Fig. 1(d). It was made reconfigurable by integrating two PIN diodes (M/A-COM CPINUC5206-HF), labeled as PIN_1 and PIN_2, between the exciting strips on Sub_3 as shown in Fig. 1(d). There are three surface mounted Murata 100 nH inductors also introduced into the driving structure to prevent any RF signals from entering the bias network. Three small holes, each with a 0.8 mm radius, were drilled in the ground disc (xoy-plane). They are used to provide the routing path from below the ground disc for three dc wires. When PIN_1 is on and PIN_2 is off, the electric radiator is excited and the monopole-like pattern is produced. This state is donated as State 1. On the other hand, when PIN_1 is off and PIN_2 is on, the magnetic radiator is excited and the broadside pattern is generated. This state is donated as State 2. The relationships between the states of the PIN diodes and the corresponding two radiation states of the compact antenna are summarized in Table II.

TABLE I. Optimized Design Parameters of the Optimized Antenna (All Dimensions are in Millimeters)

$h_1 = 13.8$	$h_2 = 2.0$	$h_3 = 0.508$	$h_4 = 15.4$	$h_5 = 1.0$
$h_6 = 19.8$	$h_7 = 0.8$	$L_1 = 3.0$	$L_2 = 3.6$	$L_3 = 2.0$
$L_4 = 2.6$	$L_5 = 2.0$	$L_6 = 5.0$	$L_7 = 7.0$	$L_8 = 16$
$L_9 = 9.0$	$L_{10} = 2.0$	$L_{11} = 2.0$	$W_1 = 2.0$	$W_2 = 3.0$
$W_3 = 3.0$	$W_4 = 2.3$	$R_1 = 96$	$R_2 = 21$	$R_3 = 20.7$
$R_4 = 15.5$	$R_5 = 20$	$d_1 = 1.6$	*null*	

TABLE II. The Relationships between the States of the PIN Diodes and the Radiation States of the Prototype Antenna

State	PIN_1	PIN_2	Pattern Type
1	ON (1V)	OFF (N/A)	Monopole-Like
2	OFF (N/A)	ON (1V)	Broadside

III. Design Principles

A. Curved Egyptian-Axe Shaped Monopole Radiator

The curved Egyptian-axe shaped monopole is excited when the reconfigurable antenna operates in State 1. The effect of the two horizontal arms on the monopole's performance was parametrically studied by varying two of its design parameters, the inner radius R_5 and the arm length L_7. As illustrated in Fig. 2, the monopole resonance frequency witnesses a red-shift and the impedance matching level improves as R_5 becomes larger. The

same behavior occurs as L_7 increases, i.e., the resonance frequency red-shifts and the impedance matching improves. The presence of the two horizontal arms significantly benefits the monopole element. It not only reduces its electrical size, but it also improves its impedance matching.

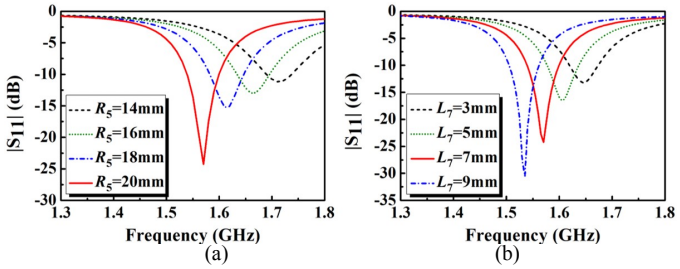

Fig. 2 The EAD monopole radiator (State 1 of the reconfigurable antenna). The $|S_{11}|$ values as functions of the source frequency (a) as the inner radius, R_5, varies (left) and (b) as the length of its horizontal arms, L_7, varies (right).

B. Hybrid Design of NFRP CLL Element and Rectangular Strips

The CLL-based, magnetic NFRP antenna, which was introduced in [22, 23], was selected as the initial design of the magnetic radiator. The original design only utilized the driven vertical strip shown on the left side of the CLL. Its loop current behavior is illustrated in Fig. 3(a). However, this original design does not have the maximum of its dipole pattern along the vertical direction, but rather it is directed away from it towards the side opposite the driven strip [22-24]. The maximum directivity in the E-plane of the example is tilted 10° away from the broadside direction as illustrated in Fig. 3(c). It was determined that by adding the symmetrically placed parasitic rectangular strip of the same dimensions to the system, the current density becomes more uniform on the CLL element as shown in Fig. 3(b). The currents induced on the parasitic strip are out-of-phase to the driven strip. This behavior compensates for the tilt and the modified system radiates the pattern shown in Fig. 3(d), which has its maximum along the vertical (broadside) direction.

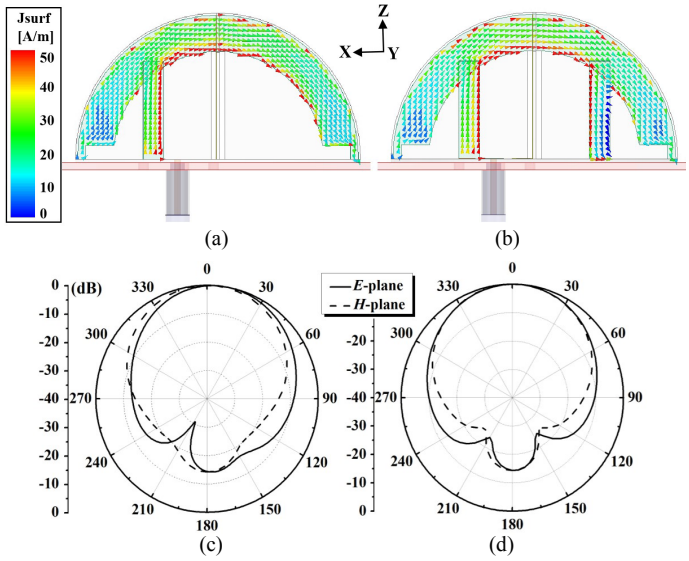

Fig. 3 The CLL-based magnetic radiator design (State 2 of the reconfigurable antenna). The current density distributions on the metallic surfaces of the magnetic radiator at its resonance frequency, 1.57 GHz, (a) without and (b) with the parasitic rectangular strip being present. The corresponding E- and H-plane radiation patterns (c) without and (d) with it.

Because of its symmetric presence, the parasitic strip also increases the null depth of the monopole-like radiation pattern in State 1. As shown in Fig. 4(a), the monopole induces strong currents on the magnetic radiator's components on Sub_2 when the reconfigurable compact antenna operates in State 1 without the parasitic strip being present. These induced currents are not symmetrically balanced on them in the absence of the parasitic strip. The net result is a tilt of the null direction away from the broadside direction (+z axis) by 1°, and the depth of its null is only -26 dB as shown in Fig. 4(c). On the other hand, when the parasitic strip is present, the symmetry of the induced current distributions on the CLL elements is well recovered as illustrated in Fig. 4(b). As a consequence, the null direction is now strictly pointed along the boresight direction and its null depth reaches -33 dB, as shown in Fig. 4(d). Thus, the parasitic strip facilitates a 7 dB null depth improvement.

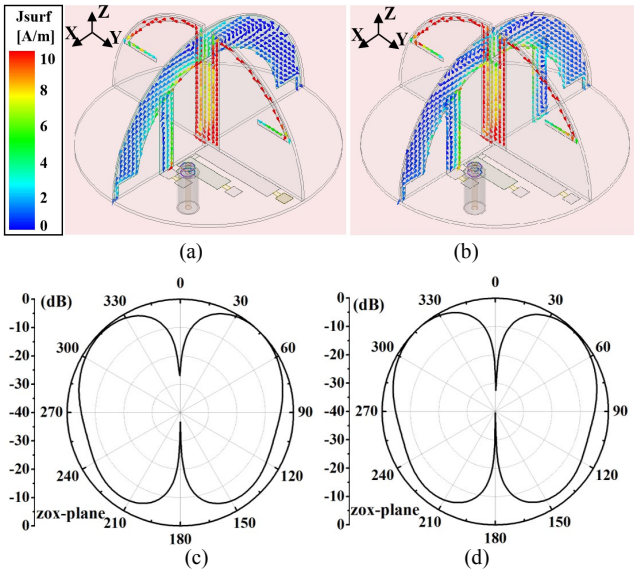

Fig. 4 Characteristic features of the reconfigurable antenna operating in its State 1 at the resonance frequency, 1.57 GHz. The current distributions on the radiating elements (a) without and (b) with the parasitic strip being present. The corresponding radiation pattern in the zox-plane, i.e., the plane in which the magnetic radiator lies, (c) without and (d) with it.

IV. Measured Results

The optimized prototype of the reconfigurable compact antenna was fabricated and tested. Photos of the fabricated prototype are given in Fig. 5. The three dc bias lines are connected to the positive side of the PIN diodes as shown in Fig. 5. They are fed 1V from a voltage-stabilized power supply to control the ON/OFF states of the PIN diodes.

The $|S_{11}|$ values when the prototype was operating in State 1 and State 2 were measured using an Agilent E5063A PNA vector network analyzer (VNA). The simulated and measured $|S_{11}|$ values of these two states are presented in Fig. 6(a). The simulated −10-dB fractional bandwidth of State 1 is 3.8% (from 1.54 to 1.60 GHz) while its measured value was 7.6% (from 1.51 to 1.63 GHz). The simulated fractional bandwidth of State 2 is 2.5% (from 1.55 to 1.59 GHz) while its measured value was 3.8% (from 1.54 to 1.60 GHz). The measured (simulated) overlapped operational fractional bandwidth of the two states is

3.8% (2.5%). The measured bandwidth values were larger than the simulated ones. This is a consequence of fabrication errors, which led to the higher than expected losses noted below.

As depicted in Fig. 5, the far-field radiation performance was measured in a SATIMO passive measurement system (0.8–6 GHz) with an Agilent N5230A PNA-L VNA [26]. The measured and simulated realized gain values at boresight of both states are presented in Fig. 6(b). In State 1, the measured (simulated) realized gain at boresight was ~ −28 dBi (~ −31 dBi) and the total efficiency was 75% (92%). In State 2, the measured (simulated) realized gain at boresight was ~ 7.1dBi (~ 7.1 dBi) and the total efficiency was 80% (87%). As a consequence, the gain difference is almost 33 dB (36 dB) over the operational band.

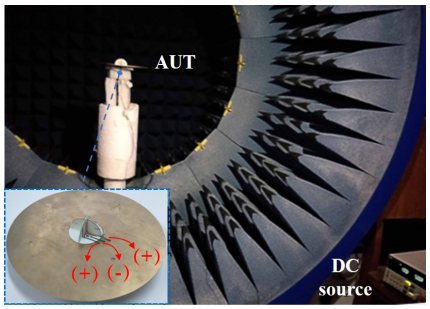

Fig. 5 Reconfigurable antenna prototype as the AUT in the anechoic chamber.

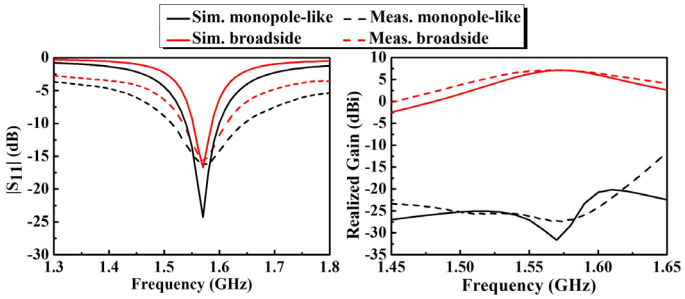

Fig. 6 Simulated and measured results of the two operating states of the reconfigurable antenna as functions of the source frequency. (a) $|S_{11}|$ values. (b) Realized gain values at boresight.

The measured (simulated) 2D normalized realized gain patterns in the zox-plane and zoy-plane at the resonance frequency, 1.57 (1.57) GHz, of the two states are presented in Fig. 7. It is readily seen that good monopole-like and broadside radiation patterns were achieved in both states and the associated cross polarization levels were low.

To emphasize the efficacy of our work, Table Ⅲ compares the prototype's performance characteristics with those of previously reported pattern-reconfigurable antennas with broadside and monopole-like radiation pattern diversity. Note that the total electrical size of each design's main radiators corresponds to the center frequency of its −10-dB impedance bandwidth. These comparisons demonstrate that the prototype has several notable advantages. It is simple, utilizes the least number of PIN diodes, has the smallest ka_{rad}, and has the largest difference between the broadside gain maximum and the null depth. While it has narrow bandwidth because of its small electrical size [24], its compactness, efficiency, and reconfigurability features are attractive for many existing and aspirational, narrowband, space-limited wireless applications including indoor wireless communications, GPS, and high-density MIMO systems.

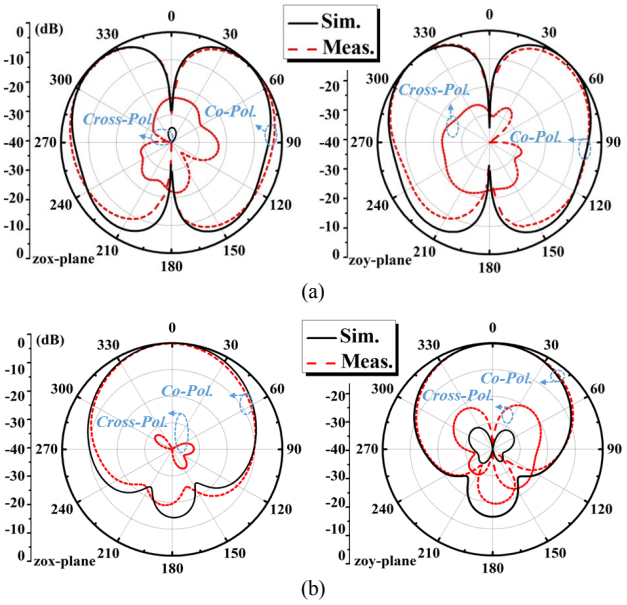

Fig. 7 Simulated and measured normalized realized gain patterns in the *zox*- and *zoy*-planes at the resonance frequency of both states, 1.57 GHz. (a) State 1. (b) State 2.

TABLE III. COMPARISONS OF THE PERFORMANCE CHARACTERISTICS OF THE PROTOTYPE RECONFIGURABLE ESA WITH RELATED ANTENNAS REPORTED IN THE LITERATURE *

Refs.	ka_{rad}	FBW (%)	Total Effi. (%)	Cross-Pol Level (dB)	Number of Switches	Broadside gain max (dBi), null depth (dB) (difference)
[5]	2.01	2.5	86, 82	-18, -20	16	6, -25 (31)
[9]	3.31	23.5	66, 75	-25, -30	4	8.2, -21 (29.2)
[11]	2.35	7.8	78, 82	-25, -28	12	8.5, -11 (19.5)
[17]	2.98	9.0	NA	NA	2	4.1, -4.0 (8.1)
[18]	1.77	11.0	NA	-20,-15	4	7.7, -20 (27.7)
Rep. Ant.	0.69	3.8	80, 75	-40, -25	2	7.1, -28 (35.1)

* The values of the total efficiency and the cross-polarization level are for the first broadside mode and the second monopole-like mode, respectively.

V. CONCLUSION

This letter presented a reconfigurable antenna that dynamically produces either a broadside or a monopole-like pattern. The combination of its main radiating elements is compact, ka_{rad} = 0.69. The two states of the system are controlled with two PIN diodes that are integrated into a simple excitation structure. The magnetic radiator is based on a modification of the CLL-based NFRP antenna. When it is excited, the broadside radiation pattern is obtained. When the electric radiator, an EAD-based monopole antenna, is excited, the monopole-like radiation pattern is obtained. The pattern has a very deep null depth at boresight. A prototype was realized and tested. The measured overlapping operational fractional bandwidth of the two states is 3.8% and the measured gain difference at boresight between them is over 35 dB. Moreover, the prototype exhibited a high radiation efficiency (> 75%) and realized symmetric and stable radiation patterns in both states.

References

[1] Z.-W. Yu, G.-M. Wang, and C.-X. Zhang, "A broadband planar monopulse antenna array of C-band," *IEEE Antennas Wireless Propag. Lett.*, vol. 8, pp. 1325-1328, 2009.

[2] Y. J. Cheng, W. Hong, and K. Wu, "94 GHz substrate integrated monopulse antenna array," *IEEE Trans. Antennas Propag.*, vol. 60, no. 1, pp. 121–129, Jan. 2012.

[3] K. Tekkouk, M. Ettorre, L. L. Coq, and R. Sauleau, "SIW pillbox antenna for monopulse radar applications," *IEEE Trans. Antennas Propag.*, vol. 63, no. 9, pp. 3918-3927, Sep. 2015.

[4] M. J. Li, R. Ma, and N. Behdad, "A compact, low-cost, ultrawideband direction-finding system," *IEEE Antennas & Propag. Mag.,* pp. 32-44, Dec. 2018.

[5] Y. Yang , R. B. V. B. Simorangkir, X. Zhu, K. Esselle, and Q. Xue , "A novel boresight and conical pattern reconfigurable antenna with the diversity of 360° polarization scanning," *IEEE Trans. Antennas Propag.*, vol. 65, no. 11, pp. 5747-5756, Nov. 2017.

[6] L. Cui, W. Wu, and D.-G. Fang, "Wideband circular patch antenna for pattern diversity application," *IEEE Antennas Wireless Propag. Lett.*, vol. 14, pp. 1298-1301, 2015.

[7] Z.-C. Hao, H.-H. Wang, and W. Hong, "A novel planar reconfigurable monopulse antenna for indoor smart wireless access points' application," *IEEE Trans. Antennas Propag.*, vol. 64, no. 4, pp. 1250–1256, Apr. 2011.

[8] L. Sun, G.-X. Zhang, B.-H. Sun, W.-D. Tang, and J.-P. Yuan, "A single patch antenna with broadside and conical radiation patterns for 3G/4G pattern diversity," *IEEE Antennas Wireless Propag. Lett.*, vol. 15, pp. 433-436, 2016.

[9] W. Lin, H. Wong, and R. W. Ziolkowski, "Wideband pattern-reconfigurable antenna with switchable broadside and conical beams," *IEEE Antennas Wireless Propag. Lett.*, vol. 16, pp. 2638-2641, 2017.

[10] C. J. Deng, Y. Li, Z. J. Zhang, and Z. H. Feng, "A hemispherical 3-D null steering antenna for circular polarization," *IEEE Antennas Wireless Propag. Lett.*, vol. 14, pp. 803-806, 2015.

[11] W. Lin , H. Wong, and R. W. Ziolkowski, "Circularly polarized antenna with reconfigurable broadside and conical beams facilitated by a mode switchable feed network," *IEEE Trans. Antennas Propag.*, vol. 66, no. 2, pp. 996-1001, Feb. 2018.

[12] Y. D. Dong, J. Choi, and T. Itoh, "Vivaldi antenna with pattern diversity for 0.7 to 2.7 GHz cellular band applications," *IEEE Antennas Wireless Propag. Lett.*, vol. 17, no. 2, pp. 247-250, Feb. 2018.

[13] H. Zhong, Z. J. Zhang, W. H. Chen, Z. H. Feng, and M. F. Iskander, "A tripolarization antenna fed by proximity coupling and probe," *IEEE Antennas Wireless Propag. Lett.*, vol. 8, pp. 465-467, 2009.

[14] P.-Y. Qin, Y. J. Guo, A. R. Weily, and C.-H. Liang, "A pattern reconfigurable U-slot antenna and its applications in MIMO systems," *IEEE Trans. Antennas Propag.*, vol. 60, no. 2, pp. 516-528, Feb. 2012.

[15] Y. B. Wen , D. Q. Yang, H. L. Zeng, M. Zou, and J. Pan, "Bandwidth enhancement of low-profile microstrip antenna for MIMO applications," *IEEE Trans. Antennas Propag.*, vol. 66, no. 3, pp. 1064-1075, Mar. 2018.

[16] S.-H. Chen, J.-S. Row, and K.-L. Wong, "Reconfigurable square-ring patch antenna with pattern diversity," *IEEE Trans. Antennas Propag.*, vol. 55, no. 2, pp. 472-475, Feb. 2007.

[17] I. Lim and S. Lim, "Monopole-like and boresight pattern reconfigurable antenna," *IEEE Trans. Antennas Propag.*, vol. 61, no. 2, pp. 5854-5859, Dec. 2013.

[18] X. X. Ding, Z. Q. Zhao, Y. H. Yang, Z. P. Nie, and Q. H. Liu, "A low-profile and stacked patch antenna for pattern-reconfigurable applications," *IEEE Trans. Antennas Propag.*, vol. 67, no. 7, pp. 4830-4835, Jul. 2019.

[19] S.-A. Malakooti, M. Moosazadeh, D. C. Ranasinghe, and C. Fumeaux, "Antipodal vivaldi antenna for sum and difference radiation patterns with reduced grating lobes," *IEEE Antennas Wireless Propag. Lett.*, vol. 16, pp. 3139-3142, 2017.

[20] S.-A. Malakooti and C. Fumeaux, "Multi-element Vivaldi antenna with sum and difference radiation patterns," in *Proc. 2018 IEEE Asia-Pacic Conference on Antennas and Propagation* (*APCAP*), Auckland, New Zealand, Aug. 2018, pp. 34-35.

[21] S.-A. Malakooti, S. M. H. Mousavi, and C. Fumeaux, "Tunable bandpass-to-bandstop quasi Yagi-Uda antenna with sum and difference radiation patterns," *IEEE Trans. Antennas Propag.,* vol. 67, no. 4, pp. 2260-2271, Apr. 2019.

[22] P. Jin and R. W. Ziolkowski, "Multi-frequency, linear and circular polarized, metamaterial-inspired, near-field resonant parasitic antennas," *IEEE Trans. Antennas Propag.,* vol. 59, no. 5, pp. 1446-1459, May 2011.

[23] M.-C. Tang, R. W. Ziolkowski, S. Q. Xiao, M. Li, and J. R. Zhang, "Frequency-agile, efficient, near-field resonant parasitic monopole antenna," *IEEE Trans. Antennas Propag.*, vol. 62, no. 3, pp. 1479-1483, Mar. 2014.

[24] R. W. Ziolkowski, P. Jin, and C.-C. Lin, "Metamaterial-inspired engineering of antennas," *Proc. IEEE,* vol. 99, no. 10, pp. 1720–1731, Oct. 2011.

[25] C. A. Balanis, *Antenna Theory Analysis and Design*, 4th ed. Hoboken, NJ, USA Wiley, 2016, Sec. 6.2.

[26] StarLab Version D User Guide 1.0, Reference: TD. 224.1.08. SATF. A, SATIMO Corp., France, 2.